

A note on Stokes' problem in dense granular media using the $\mu(I)$ -rheology

J. John Soundar Jerome^{1,†} and B. Di Pierro¹

¹Université de Lyon, Université Claude Bernard Lyon 1, Laboratoire de Mécanique des Fluides et d'Acoustique, CNRS UMR–5509, Boulevard 11 novembre, 69622 Villeurbanne CEDEX, Lyon, France

(Received 15 September 2017; revised 18 January 2018; accepted 16 March 2018;
first published online 23 May 2018)

The classical Stokes' problem describing the fluid motion due to a steadily moving infinite wall is revisited in the context of dense granular flows of mono-dispersed beads using the recently proposed $\mu(I)$ -rheology. In Newtonian fluids, molecular diffusion brings about a self-similar velocity profile and the boundary layer in which the fluid motion takes place increases indefinitely with time t as $\sqrt{\nu t}$, where ν is the kinematic viscosity. For a dense granular viscoplastic liquid, it is shown that the local shear stress, when properly rescaled, exhibits self-similar behaviour at short time scales and it then rapidly evolves towards a steady-state solution. The resulting shear layer increases in thickness as $\sqrt{\nu_g t}$ analogous to a Newtonian fluid where ν_g is an equivalent granular kinematic viscosity depending not only on the intrinsic properties of the granular medium, such as grain diameter d , density ρ and friction coefficients, but also on the applied pressure p_w at the moving wall and the solid fraction ϕ (constant). In addition, the $\mu(I)$ -rheology indicates that this growth continues until reaching the steady-state boundary layer thickness $\delta_s = \beta_w(p_w/\phi\rho g)$, independent of the grain size, at approximately a finite time proportional to $\beta_w^2(p_w/\rho g d)^{3/2}\sqrt{d/g}$, where g is the acceleration due to gravity and $\beta_w = (\tau_w - \tau_s)/\tau_s$ is the relative surplus of the steady-state wall shear stress τ_w over the critical wall shear stress τ_s (yield stress) that is needed to bring the granular medium into motion. For the case of Stokes' first problem when the wall shear stress τ_w is imposed externally, the $\mu(I)$ -rheology suggests that the wall velocity simply grows as \sqrt{t} before saturating to a constant value whereby the internal resistance of the granular medium balances out the applied stresses. In contrast, for the case with an externally imposed wall speed u_w , the dense granular medium near the wall initially maintains a shear stress very close to τ_d which is the maximum internal resistance via grain–grain contact friction within the context of the $\mu(I)$ -rheology. Then the wall shear stress τ_w decreases as $1/\sqrt{t}$ until ultimately saturating to a constant value so that it gives precisely the same steady-state solution as for the imposed shear-stress case. Thereby, the steady-state wall velocity, wall shear stress and the applied wall pressure are related as $u_w \sim (g\delta_s^2/\nu_g)f(\beta_w)$ where $f(\beta_w)$ is either $O(1)$ if $\tau_w \sim \tau_s$ or logarithmically large as τ_w approaches τ_d .

Key words: boundary layer structure, granular media, non-Newtonian flows

† Email address for correspondence: john-soundar@univ-lyon1.fr

1. Introduction

Flowing matter containing a dense collection of grains like sand, gravel, cereals, sugar, etc. is ubiquitous in nature as well as in many industrial processes. Such granular media exist in various states at any given common flow situation depending strongly on the energy supplied by external deformation and/or shear stresses (Jaeger, Nagel & Behringer 1996). And so, they show a very rich phenomenology (Liu & Nagel 1998; Gray, Tai & Noelle 2003; Aranson & Tsimring 2006): a gaseous regime wherein the flow is very rapid and dilute, and the particles interact by collision (Jenkins & Savage 1983), and a quasi-static regime in which the material deformation is extremely slow wherein frictional contacts between particles dominate the rheology, as is often the case in soil mechanics (Hutter & Rajagopal 1994). Indeed, there exists an intermediate regime in the presence of both collisions and friction that result in huge dissipation. Here, a dense granular medium behaves like a viscoplastic liquid (Forterre & Pouliquen 2008; Andreotti, Forterre & Pouliquen 2011). A decade ago, generalising the scalar rheology of Midi (2004), Jop, Forterre & Pouliquen (2006) proposed the so-called $\mu(I)$ -rheology to describe such a dense granular liquid state. It has since been well exploited, often via direct numerical simulations, to study and model many common flow configurations (Kamrin 2010; Cawthorn 2011; Lagr e, Staron & Popinet 2011; Staron, Lagr e & Popinet 2012; Chauchat & M edale 2014; Gray & Edwards 2014; Baker, Barker & Gray 2016).

However, recent works by Barker *et al.* (2015), Goddard & Lee (2017) and Martin *et al.* (2017) illustrate that the governing equations of the $\mu(I)$ -rheology can exhibit ill-posed behaviour in the parameter range corresponding to quasi-gaseous and quasi-static regimes, respectively. Joseph & Saut (1990) showed that ill-posed problems suffer from the so-called Hadamard instability and they characterised the ill-posedness through a stability analysis that identifies exponential temporal growth of short-wavelength perturbations. As a consequence, grid-dependent numerical results may not converge as the spatial refinement is enhanced for these cases (see Joseph & Saut 1990, p. 224). In particular, Barker *et al.* (2015) demonstrated both theoretically and numerically the governing equations of the $\mu(I)$ -rheology are Hadamard unstable even for the simple case of Bagnold flow. More recently, Martin *et al.* (2017) also observed it in their numerical simulations for the case of granular column collapse on inclined channels. Nonetheless novel attempts to regularise the governing equations via a proper functional form of $\mu(I)$, at least in the quasi-static regime, have already been proposed by Barker & Gray (2017) and Barker *et al.* (2017). They successfully simulated granular roll waves in two dimensions and it now remains to see if their regularisation is valid also in direct computations of other unsteady granular flows.

In this context, this work aims to determine, both numerically and theoretically, the time evolution characteristics of the unsteady, non-uniform velocity and shear-stress fields arising in the $\mu(I)$ -rheology for a canonical flow situation, namely, the so-called Stokes' first problem (Stokes 1851) of the fluid motion that is brought about by impulsively starting an infinite wall. Unlike the classical case, the granular medium is placed underneath the plate (see figure 1). It is the simplest unsteady parallel flow in which some important features of fluid flows, such as transverse momentum transfer and the resulting boundary layer development due to direct balance between local fluid acceleration and the friction forces, can be treated. It is also known as the dragged-plate problem in Andreotti *et al.* (2011) and Cawthorn (2011), where only a steady-state analytical solution can so far been found. The objective of the present work is to treat the transient solution and its characteristics.

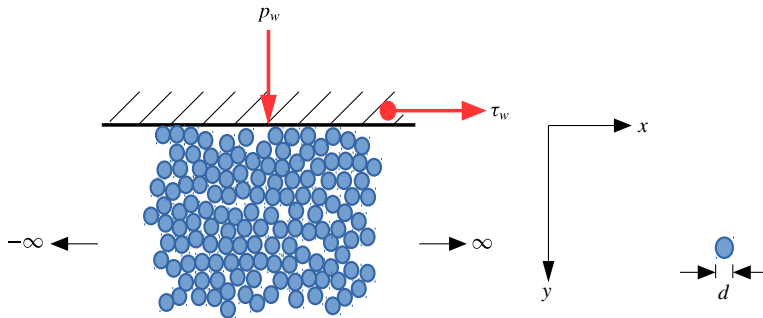


FIGURE 1. (Colour online) Schematic of the problem: an impulsively started, infinitely long flat plate over a semi-infinite dense granular medium consisting of mono-dispersed spherical grains.

Note that there has been a steady interest in Stokes' first problem for non-Newtonian fluids, in particular, viscoelastic fluids (see Morrison 1956; Tanner 1962; Preziosi & Joseph 1987; Devakar & Iyengar 2008, 2009). Similarly, Stokes' second problem (Panton 1968; Schlichting 1968), which considers the time evolution of the velocity field due to a horizontally oscillating infinite flat plate, has recently been studied for viscoelastic fluids by Devakar & Iyengar (2008). Its applications include high-frequency microfluidics (Yakhot & Colosqui 2007; Ekinci, Karabacak & Yakhot 2008) for viscoelastic materials and rheometers for viscoplastic (Balmforth, Forterre & Pouliquen 2009) and power law fluids (Pritchard, McArdle & Wilson 2011). Recent literature also considers a third type of Stokes' problem wherein a transient velocity field is set up by suddenly applying a body force to a fluid that is initially at rest. In fact, for a granular medium, Jop, Forterre & Pouliquen (2007) used this configuration to numerically validate their proposed $\mu(I)$ -rheology. This was later referred to as Stokes' third problem by Ancy & Bates (2017) for a Herschel–Bulkley material and interestingly, for the numerical resolution, the authors resorted to a Stefan problem, with a moving interface (boundary condition) that separates the sheared and unsheared regions.

The constitutive laws for many non-Newtonian fluids are often nonlinear but they can be simplified in the case of Stokes' problems. The yield stress of the granular material varies in space since the $\mu(I)$ -rheology proposes a constitutive law for dense granular flows wherein the medium behaves like a viscoplastic liquid with the local viscosity nonlinearly related to the local strain rate as well as the local pressure. Moreover, care should be taken to express a well-posed initial-value problem using the $\mu(I)$ -rheology to avoid Hadamard instability. Finally, it is only recently that dense granular flows have been successfully studied using a continuum model, so the governing equations have so far been unexplored even for Stokes' first problem. In addition, apart from the simple case of steady Bagnold flow over an inclined plane, the constant shear flow case, and the steady-state solution of Stokes' first problem (Andreotti *et al.* 2011; Cawthorn 2011), there exist only a few analytical results describing unsteady dense granular flows (see the notable recent exception of Capart, Hung & Stark (2015), who gave entrainment rates in the case of transient heap flows from the depth-integrated layer dynamics assuming a local $\mu(I)$ -rheology). Therefore, this brief note is aimed at bringing out the key features of this canonical problem as predicted by the $\mu(I)$ -rheology.

The article is structured as follows. Firstly, the governing equations are shown to result in a single nonlinear shear-stress diffusion equation. Its numerical solution is then computed for the case when the wall shear stress is imposed while letting the wall velocity develop with time. Some approximate unsteady solutions are obtained and compared with computations. Finally, a brief note on Stokes' first problem with imposed wall speed is given.

2. Governing equations

2.1. Constitutive laws: $\mu(I)$ -rheology

Analogous to Coulomb's friction law, using dimensional arguments, experiments and numerical simulations, Iordanoff & Khonsari (2004), Midi (2004) and Da Cruz *et al.* (2005) demonstrated that the shear stress τ is proportional to the normal stress P for two-dimensional (2-D) dense granular flows of rigid particles so that $\tau = \mu(I)P$ where the local friction coefficient μ is only a function of a dimensionless parameter called the inertial number $I = \dot{\gamma}d/\sqrt{P/\rho}$. Here, $\dot{\gamma}$ is the local shear rate which is related to the macroscopic time scale of the granular flow and $d\sqrt{\rho/P}$ is the microscopic time scale corresponding to any local rearrangement of grains of diameter d and density ρ subjected to a local normal stress P . Note that I is also the square root of the Savage or the Coulomb number as used in Savage (1984) or Ancey, Coussot & Evesque (1999), respectively. In general, the dimensionless local friction coefficient is given by (Midi 2004; Jop *et al.* 2006)

$$\mu(I) = \mu_s + \frac{\mu_d - \mu_s}{\left(1 + \frac{I_0}{I}\right)}, \quad (2.1)$$

whereby μ saturates towards two fundamental constants for a dense granular medium μ_s or μ_d depending respectively on the inertial number $I \ll 1$ (quasi-static regime) or $I \gg 1$ (kinetic or gaseous regime). Jop *et al.* (2006) proposed a 3-D generalisation of this scalar constitutive relation for a granular material by decomposing the Cauchy stress tensor into an isotropic contribution from the local pressure p and a traceless deviatoric stress tensor τ_{ij} while assuming that τ_{ij} is aligned with the strain rate tensor $\dot{\gamma}_{ij} = 1/2(\partial_i u_j + \partial_j u_i)$ (where u_i represent components of the velocity field). So, if \mathbf{x} is the position vector and t represents time, then the Cauchy stress tensor

$$\sigma_{ij}(\mathbf{x}, t) = -p(\mathbf{x}, t)\delta_{ij} + \tau_{ij}(\mathbf{x}, t), \quad (2.2)$$

where δ_{ij} is the Kronecker delta and $\tau_{ij}(\mathbf{x}, t) = \eta(\mathbf{x}, t)\dot{\gamma}_{ij}(\mathbf{x}, t)$ and the local granular liquid viscosity

$$\eta = \frac{\mu p}{|\dot{\gamma}|}, \quad (2.3)$$

is, thereby, a nonlinear function of the local pressure p and the local second invariant of the strain rate tensor $|\dot{\gamma}| = \sqrt{1/2\dot{\gamma}_{ij}\dot{\gamma}_{ij}}$ via the local friction coefficient given by (2.1) and the inertial number for the 3-D case

$$I = \frac{|\dot{\gamma}|d}{\sqrt{p/\rho}}. \quad (2.4)$$

In addition, the solid volume fraction ϕ is also a linear function of I (see Andreotti *et al.* 2011, p. 238) but, in general, it varies very little and so, for the sake of simplicity, it is taken to be a constant in the following.

2.2. Stokes' first problem and its steady-state solution

Consider an infinite rigid flat plate placed at rest ($t=0$) on top of a semi-infinite dense granular medium. As illustrated in figure 1, the plate is set in motion impulsively at $t > 0$ by applying a tangential shear stress τ_w (along the x -direction) in the presence of a normal stress p_w (along the y -direction). It is then natural to restrict the analysis to two dimensions. In fact, the absence of any horizontal length scale implies that the flow properties should depend only on y and t . Incompressibility and the initial condition then imply that the vertical velocity is uniformly zero for all $t \geq 0$. And so the only non-zero components of the strain rate tensor are $\dot{\gamma}_{xy} = \dot{\gamma}_{yx} = (\partial u / \partial y) / 2$, where u is the x -component of the velocity field. Therefore, the 2-D shear-stress tensor is completely determined by a single scalar shear field $\tau = \mu p$ so that the x and y momentum equations become, respectively,

$$\phi \rho \frac{\partial u}{\partial t} = -\frac{\partial}{\partial y}(\mu p), \quad (2.5)$$

$$\frac{\partial p}{\partial y} = \phi \rho g, \quad (2.6)$$

where g is the acceleration due to gravity. Initially the granular medium is at rest ($u(y, t=0) = 0$) but a static granular material can support a wide variety of shear-stress and pressure distributions so long as the yield stress is not exceeded so that $\tau \leq \mu_s p$. Within the context of the $\mu(I)$ -rheology, the only possible configuration where the granular liquid is at rest corresponds to the case $\tau = \mu_s p$. For all other static states, the constitutive law $\tau = \mu p$ is violated, so the $\mu(I)$ -rheology is no longer applicable. Therefore, in the following, the initial conditions correspond to a specific static state wherein the shear stress equals the yield stress throughout the granular medium

$$\tau(y, t=0) = \mu_s p, \quad (2.7)$$

with p the hydrostatic pressure. Whereas the boundary conditions for all $t > 0$ are

$$p(y=0, t) = p_w, \quad (2.8)$$

$$\mu(y=0, t) = \frac{\tau_w}{p_w} = \mu_w, \quad (2.9)$$

along with the condition that the grains sufficiently far from the plate remain static, i.e. $u(y = \infty, t) = 0$, and so $\mu = \mu_s$ at $y = \infty$. In contrast to the classical Stokes' problem (Stokes 1851) for a Newtonian fluid, firstly, the frictional force (right-hand side of equation (2.5)) is not only non-uniform due to the hydrostatic pressure $p(y) = p_w + \phi \rho g y$ but also nonlinear since μ depends on both $p(y)$ and $\partial u / \partial y$ via (2.1). And secondly, there exists a non-trivial steady-state solution wherein the shear stress is constant throughout the medium such that $\mu p = \tau_w = \mu_w p_w$, as already shown in Andreotti *et al.* (2011, pp. 254–256) and Cawthorn (2011, pp. 46–50). Since $\mu \in [\mu_s, \mu_d]$ and $p(y)$ increases linearly with the depth y , it follows that

$$\mu = \frac{\mu_w}{1 + (\phi \rho g y / p_w)}, \quad (2.10)$$

for all $y \leq \delta_s$ and $\mu = \mu_s$ otherwise; here, the critical depth δ_s is given by

$$\delta_s = \beta_w \left(\frac{p_w}{\phi \rho g} \right), \quad (2.11)$$

with $\beta_w = (\mu_w/\mu_s - 1)$. This denotes the depth beyond which the granular medium does not flow $y \geq \delta_s$. Note that the term β_w represents the surplus in wall shear stress over the yield criterion at the wall. The steady-state solution (2.10) can be used to obtain the corresponding velocity profile. As previously shown by Cawthorn (2011, pp. 46–50), the resulting relation between the wall velocity (if the no-slip condition is allowed) and the shear layer thickness compares qualitatively well with the molecular dynamic simulations of Thompson & Grest (1991).

2.3. Stokes' first problem: shear-stress diffusion equation

Most numerical studies obtain the velocity field by solving the momentum equations that account for the constitutive law (2.2). Note that the latter is coupled with the expressions for the local friction coefficient (2.1) and the inertial number I . However, it is possible to write a single equation for the shear stress in the case of Stokes' first problem within the context of the $\mu(I)$ -rheology. Since $I = -(1/2)(\partial u/\partial y)\sqrt{\rho d^2/p}$, the local friction coefficient (2.1) can be rewritten as

$$\frac{\partial u}{\partial y} = -2I_0 \sqrt{\frac{p}{\rho d^2}} \left(\frac{\mu - \mu_s}{\mu_d - \mu} \right), \quad (2.12)$$

which when differentiated with respect to time and using $\tau = \mu p$ yields

$$\frac{\partial^2 u}{\partial t \partial y} = -\frac{2\Delta\mu I_0}{d} \left(p \sqrt{\frac{p}{\rho}} \right) \frac{1}{(\mu_d p - \tau)^2} \frac{\partial \tau}{\partial t}, \quad (2.13)$$

where $\Delta\mu = \mu_d - \mu_s > 0$. By allowing $\partial^2 u/\partial y \partial t = \partial^2 u/\partial t \partial y$ and then introducing (2.5) in the above expression, this leads to a single nonlinear shear-stress diffusion equation

$$\frac{\partial \tau}{\partial t} = \left(\frac{d}{2\phi \Delta\mu I_0 \sqrt{\rho}} \right) \frac{(\mu_d p - \tau)^2}{p \sqrt{p}} \frac{\partial^2 \tau}{\partial y^2}. \quad (2.14)$$

Finally, by taking $v_g = (d/2\phi \Delta\mu I_0) \sqrt{p_w/\rho}$ as a proper diffusion coefficient and the steady-state shear-layer thickness δ_s as the characteristic length scale, the non-dimensional time and space coordinates are $\tilde{t} = v_g t/\delta_s^2$ and $\tilde{y} = y/\delta_s$, respectively. Thus, in terms of the normalised pressure $\tilde{p} = p(y)/p_w$ and shear stress $\tilde{\tau} = \tau(y, t)/\tau_w$, the above equation becomes

$$\frac{\partial \tilde{\tau}}{\partial \tilde{t}} = \frac{(\mu_d \tilde{p} - \mu_w \tilde{\tau})^2}{\tilde{p} \sqrt{\tilde{p}}} \frac{\partial^2 \tilde{\tau}}{\partial \tilde{y}^2}, \quad (2.15)$$

with boundary conditions $\tilde{\tau}(0, \tilde{t}) = \tilde{\tau}(1, \tilde{t}) = 1$ and an initial condition $\tilde{\tau}(\tilde{y}, 0) = \mu_s \tilde{p}/\mu_w$. The steady-state solution for the non-dimensional shear stress is $\tilde{\tau} = 1$. Unlike the steady-state local friction coefficient μ , the steady-state shear stress is a continuous and infinitely differentiable function for all $y \geq 0$. So, it is expected that $\tilde{\tau}$ remains smooth also for the unsteady case. In fact, the term $(\mu_d \tilde{p} - \mu_w \tilde{\tau})$ is positive-definite. Hence, it is quite straightforward to homogenise the boundary conditions and numerically solve the above equation using a second-order centred finite difference scheme for spatial derivatives and a second-order Crank–Nicolson one for temporal integration. The updated $\tilde{\tau}$ is obtained by an iterative Richardson minimal residual process.

2.4. Well-posedness of the shear-stress diffusion equation

Barker *et al.* (2015) demonstrated that the $\mu(I)$ -rheology is well-posed for intermediate values of inertial number I , but that it is ill-posed for both high and low inertial numbers. In the present case, $I \gg 1$ in the neighbourhood of the wall when either the applied wall shear τ_w is close to the critical wall shear $\tau_d = \mu_d p_w$ or when wall speed u_w is sufficiently large. In addition, there is always a zone where $I \ll 1$ (or $\mu \sim \mu_s$) since the medium is slowly moving or stationary when $y \sim \delta_s$. As already shown by Barker *et al.* (2015) this should provoke Hadamard instability (Joseph & Saut 1990) whereby infinitesimally small short-wave perturbations are amplified indefinitely. Thus, numerical solutions may not converge as the grid is refined and so, before proceeding any further, it is important to verify that the shear-stress diffusion (2.15) is indeed well-posed for all values of the inertial number I .

In fact, this nonlinear diffusion equation (2.15) is one-dimensional and when it is linearised about an arbitrary base state, as in Barker *et al.* (2015, see p. 799), the resulting dispersion equation of the normal mode analysis in the high-wavenumber limit should be

$$\lambda = -\alpha^2 \xi_y^2, \quad (2.16)$$

where λ is the complex frequency, ξ_y is the wavenumber in the \tilde{y} -direction and $\alpha = \alpha(\tilde{p}^0, \tilde{\tau}^0)$ is some function of the base state pressure \tilde{p}^0 and shear stress $\tilde{\tau}^0$. Since the real part of the complex frequency λ provides the perturbation growth rate, it is straightforward to see that (2.15) is stable for short waves along the y -coordinate.

Note that this is a one-dimensional analysis since it takes into account only plane waves along the \tilde{y} -axis in order to analyse the well-posedness of (2.15) for one-dimensional, time-dependent computations. For two-dimensional codes that consider the granular Stokes' problem as a test case, the situation is more complex. In this case, as previously shown by Barker *et al.* (2015), the equations are still ill-posed since oblique two-dimensional short waves are unstable in the region $y \sim \delta_s$ (or close to the wall for $\mu_w \sim \mu_d$).

3. Unsteady solutions and their characteristics

Figure 2 presents the results of such numerical solutions (continuous lines) for three typical values of applied wall shear stress when $\mu_s = \tan 21^\circ$ and $\mu_d = \tan 33^\circ$ (typical values for spherical mono-dispersed glass beads as in Andreotti *et al.* 2011). Each graphic (top) depicts the normalised shear stress $\tilde{\tau} = \mu \tilde{p} / \mu_w$ variation in the y -direction at various times $\tilde{t} = 10^{-4}, 10^{-3}, 10^{-2}, 10^{-1}, 10^0, 10^1$ for typical values of the normalised wall friction coefficient $(\mu_d - \mu_w) / \Delta \mu$ (where, $\Delta \mu = \mu_d - \mu_s$). In all cases, the static initial condition $\tilde{\tau}(0, \tilde{y}) = \mu_s \tilde{p} / \mu_w$ (dashed line), wherein the local shear stress is taken to be the yield criterion $\mu_s p$, evolves continuously towards the steady-state solution $\tilde{\tau} = \mu \tilde{p} / \mu_w = 1$. The spatial variation of $\tilde{\tau}$ shows that there exists a layer in which $\tilde{\tau}$ is greater than the yield stress, so the granular medium should flow in this region. If the size of this shear layer, say $\delta(\tilde{t})$, is defined as the region where $\tilde{\tau} = 0.999 \mu_s \tilde{p} / \mu_w$, figure 2 (bottom) clearly illustrates that $\delta(\tilde{t})$ increases with time as $\sqrt{\tilde{t}}$ until $\tilde{t} \sim O(1)$, after which it saturates to the steady-state limit. Therefore, it is expected from these results that, for any general μ_d and μ_s , approximate solutions to (2.15) can be obtained at both $\tilde{t} \ll 1$ and $\tilde{t} \gg 1$ by properly linearising it.

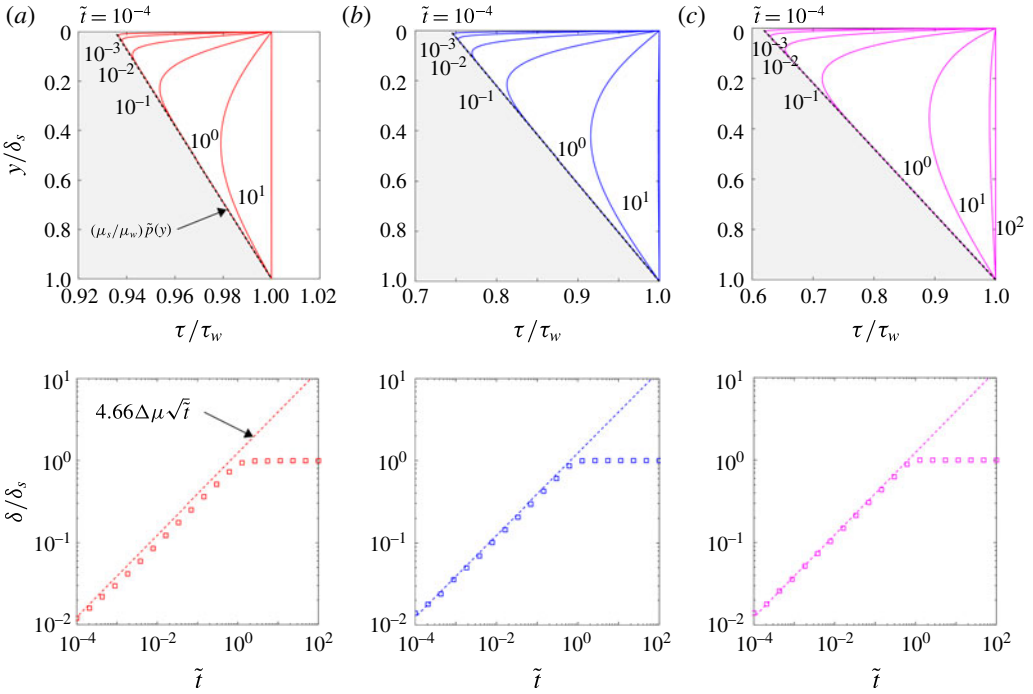


FIGURE 2. (Colour online) Temporal evolution of the normalised shear stress $\tilde{\tau} = \tau/\tau_w = \mu\tilde{p}/\mu_w$ (top) and shear layer thickness δ/δ_s (bottom) for typical values of the normalised wall friction coefficient $(\mu_d - \mu_w)/\Delta\mu$ (a) 0.9, (b) 0.5 and (c) 0.1 as computed directly using (2.15) with initial condition $\tilde{\tau}(0, \tilde{y}) = \mu_s\tilde{p}/\mu_w$ corresponding to a no-flow regime (shaded region). Note that $\Delta\mu = \mu_d - \mu_s$.

3.1. Self-similarity at $\tilde{t} \ll 1$

When $\tilde{t} \ll 1$, the non-dimensional shear layer thickness δ/δ_s is small, as observed in figure 2 (bottom). By taking the non-dimensional local pressure $\tilde{p} = 1 + \beta_w\tilde{y}$ and local shear stress $\tilde{\tau} = \mu(1 + \beta_w\tilde{y})/\mu_w$, the diffusion equation (2.15) becomes

$$\frac{\partial\mu}{\partial\tilde{t}} = (\mu_d - \mu)^2 \left(\frac{2\beta_w}{\sqrt{1 + \beta_w\tilde{y}}} \frac{\partial\mu}{\partial\tilde{y}} + \sqrt{1 + \beta_w\tilde{y}} \frac{\partial^2\mu}{\partial\tilde{y}^2} \right), \tag{3.1}$$

with $\mu(\tilde{y}, 0) = \mu_s$, $\mu(0, \tilde{t}) = \mu_w$ and $\mu(1, \tilde{t}) = \mu_s$. Note that, in general, $\beta_w < 1$ and hence, for $\tilde{t} \ll 1$, the highest-order derivative of μ should dominate if $\tilde{y} \leq \delta/\delta_s$ so that $\mu \sim \mu_w - (\mu_w - \mu_s)y/\delta$. And in the outer region, $\mu \sim \mu_s$. As the spatial variations of the local friction coefficient μ are stronger inside the shear layer (i.e. when $\beta_w\tilde{y} \ll 1$), it is reasonable to simplify (3.1) to

$$\frac{\partial\mu}{\partial\tilde{t}} = \Delta\mu^2 \frac{\partial^2\mu}{\partial\tilde{y}^2}, \tag{3.2}$$

at the leading order with the same boundary conditions as before. By taking $\psi = \mu - (\mu_w - (\mu_w - \mu_s)\tilde{y})$, the above equation admits a self-similar solution for $\psi = \psi(\eta)$

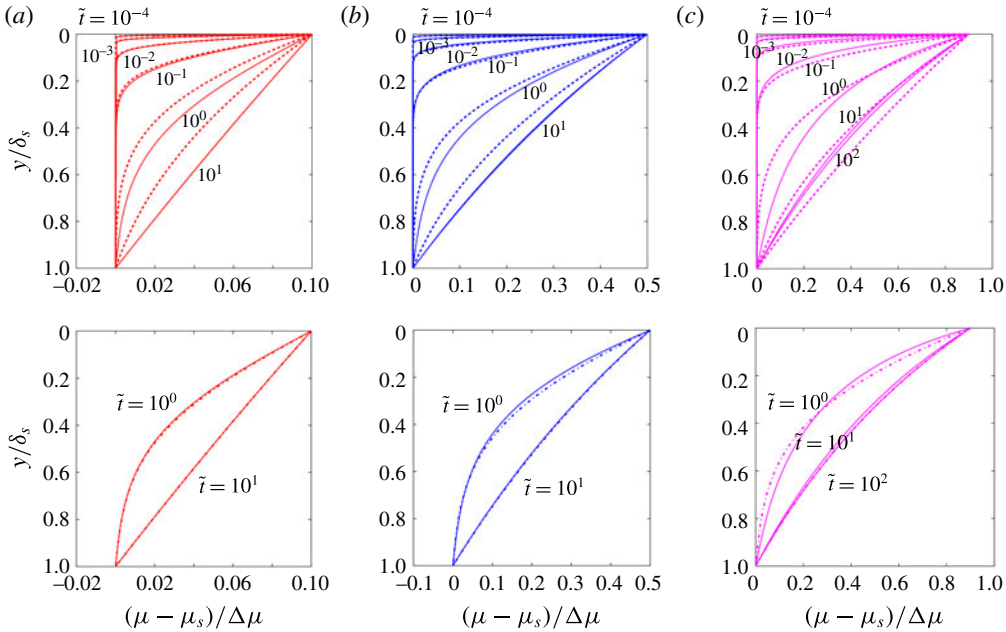


FIGURE 3. (Colour online) Comparison between self-similar approximation (top) and the long-time diffusion approximation (bottom) with the direct numerical solution (continuous lines) for various normalised wall friction coefficients $(\mu_d - \mu_w)/(\mu_d - \mu_s)$ (a) 0.9, (b) 0.5 and (c) 0.1.

with $\eta = \tilde{y}/(2\Delta\mu\sqrt{\tilde{t}})$ satisfying the initial and the boundary conditions for all $\tilde{t} \geq 0$. Thereby, the local friction coefficient is deduced to be

$$\mu \sim \mu_s + (\mu_w - \mu_s)(1 - \tilde{y}) \operatorname{erfc} \left(\frac{\tilde{y}}{2\Delta\mu\sqrt{\tilde{t}}} \right), \tag{3.3}$$

which implies that the shear layer thickness should grow as $\delta/\delta_s \sim 4.66\Delta\mu\sqrt{\tilde{t}}$.

The expression (3.3) is presented in figure 3 (top) where the time evolution of the local friction coefficient is displayed as function of \tilde{y} at different times $\tilde{t} = 10^{-4}, 10^{-3}, 10^{-2}, 10^{-1}, 10^0, 10^1$ for the same values of $(\mu_d - \mu_w)/\Delta\mu$ as in figure 2. When compared with numerical solutions of μ (and also, δ) as seen in figure 3 (top) (and figure 2, respectively), these approximations are very satisfactory for all $\tilde{t} \ll 1$. Indeed, the expression (3.3) for the local friction coefficient, and especially the estimations of the time evolution of the shear layer thickness $\delta/\delta_s \sim 4.66\Delta\mu\sqrt{\tilde{t}}$, are reasonably good even when \tilde{t} is of order 1.

3.2. Diffusion at $\tilde{t} \gg 1$

As soon as $\tilde{t} \sim O(1)$ the non-dimensional shear layer thickness is no longer small, and hence a singular perturbation of (3.1) cannot be obtained with the present scaling for the y -coordinate. However, by using the non-dimensional pressure \tilde{p} as an equivalent normalised spatial variable $\hat{y} = 1 + \beta_w\tilde{y}$, it is possible to show that

$$\frac{\partial \tilde{\tau}}{\partial \tilde{t}} = (\beta_w(\mu_d - \mu))^2 \sqrt{\hat{y}} \frac{\partial^2 \tilde{\tau}}{\partial \hat{y}^2}, \tag{3.4}$$

which is singular if $(\beta_w \Delta\mu)^2$ tends to zero. This is often true since $(\beta_w(\mu_d - \mu))^2$ is of the order of $(\beta_w \Delta\mu)^2$ and $\hat{y} \sim O(1)$. Thus, taking $\beta_w(\mu_d - \mu) \sim \beta_w \Delta\mu$ at the leading order in (3.4), it becomes linear and admits a WKB approximation in the \hat{y} -coordinate. Thereby, the local shear stress $\tilde{\tau}$ can be shown to be

$$\tilde{\tau} \sim 1 + \hat{y}^{-1/8} \sum_{m=1}^{\infty} \left[\Lambda_m \exp(-\lambda_m^2 \tilde{\tau}) \sin \left(m\pi \frac{\hat{y}^{3/4} - 1}{(\mu_w/\mu_s)^{3/4} - 1} \right) \right], \tag{3.5}$$

where

$$\Lambda_m = 2 \int_1^{\mu_w/\mu_s} \hat{y}^{1/8} \left(\frac{\mu_s}{\mu_w} \hat{y} - 1 \right) \sin \left(m\pi \frac{\hat{y}^{3/4} - 1}{(\mu_w/\mu_s)^{3/4} - 1} \right) d\hat{y}, \tag{3.6}$$

$$\lambda_m = \frac{3}{4} \frac{m\pi \beta_w \Delta\mu}{(\mu_w/\mu_s)^{3/4} - 1}. \tag{3.7}$$

Note that it is possible to solve the linearised version of (3.4) directly by separation of variables as well. In that case, the general solution is an infinite sum of Bessel functions in the \hat{y} -direction. But it is advantageous to work with the approximate solution (3.5) when m is large. Nevertheless, the comparison between the WKB approximation (3.5) (dot-dash lines in figure 3) and the numerical solution for the local friction coefficient is good. In particular, the agreement is excellent when the applied friction coefficient μ_w is close to yield friction coefficient μ_s .

3.3. Velocity field development

It is now possible to compute the temporal evolution of the velocity field using local shear stress $\tau = \mu p$. By rewriting (2.5) in terms of \tilde{t} and \tilde{y} , a natural normalisation for the velocity u can be shown to be

$$u = \tilde{u} \left(\frac{g \delta_s^2}{\beta_w \nu_g} \right), \tag{3.8}$$

where δ_s is the steady-state shear layer thickness (2.11), $\beta_w = (\mu_w - \mu_s)/\mu_s$ and $\nu_g = (d/\phi \Delta\mu I_0) \sqrt{p_w/\rho}$ is the diffusion coefficient which appears in the granular Stokes' equation (2.14). Using this normalisation and by taking

$$\tilde{\mu} = \frac{\mu_d - \mu}{\Delta\mu}, \tag{3.9}$$

the equation for the shear rate (2.12) becomes

$$\frac{\partial \tilde{u}}{\partial \tilde{y}} = -\frac{\sqrt{\tilde{p}}}{\Delta\mu} \left(\frac{1}{\tilde{\mu}} - 1 \right), \tag{3.10}$$

which can then be integrated to study the velocity field. In the following, the no-slip condition is assumed so that the wall speed and the velocity of the granular medium right next to it ($\tilde{y} = 0$) are equal.

Figure 4 compares the normalised wall velocity $\tilde{u}_w = \tilde{u}(\tilde{y} = 0, \tilde{t})$ when obtained from the numerical solution of (2.15) (filled circles), the self-similar solution (3.3) (□) and the long-time approximate solution (3.5) (+) for a given boundary condition

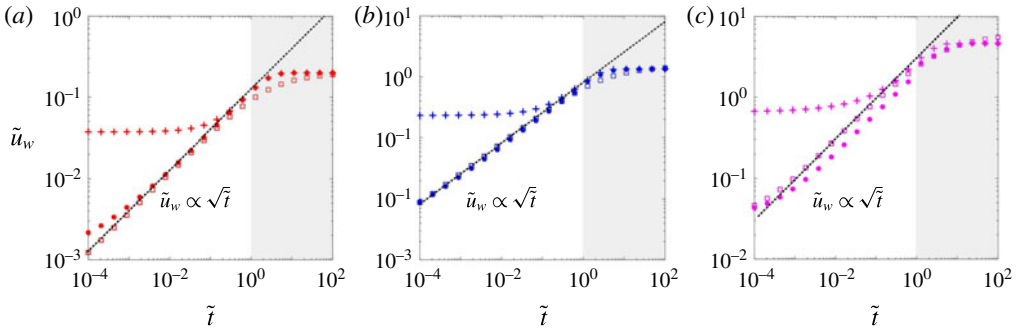


FIGURE 4. (Colour online) Normalised wall velocity as a function of the non-dimensional time \tilde{t} for various applied wall shear stresses: $(\mu_d - \mu_w)/(\mu_d - \mu_s)$ (a) 0.9, (b) 0.5 and (c) 0.1. The different symbols denote calculations from the numerical solution using (2.15) (filled circles), the self-similar solution (3.3) (\square) and the long-time approximate solution (3.5) (+).

at the wall. Each panel shows the temporal evolution of \tilde{u}_w when the wall friction coefficient is taken as $(\mu_d - \mu_w)/(\mu_d - \mu_s)$ (a) 0.9, (b) 0.5 and (c) 0.1. In all cases, the wall velocity grows monotonically by following a power law in \tilde{t} as long as $\tilde{t} \leq 1$ and then it saturates at the steady-state value $\tilde{u}_w^\infty = \tilde{u}(\tilde{y} = 0, \tilde{t} = \infty)$. Firstly, the self-similar solution (3.3) gives good qualitative agreement with the numerical results, and also, it matches well with the power law $\tilde{u}_w(\tilde{t}) \sim \sqrt{\tilde{t}}$. The long-time WKB approximation (3.5) matches very well with the numerical solution at all times $\tilde{t} > 1$. Secondly, it is observed that the steady-state wall velocity \tilde{u}_w^∞ depends largely on the imposed wall shear via $\tilde{\mu}_w = (\mu_d - \mu_w)/\Delta\mu$ as already shown by previous works (Andreotti *et al.* 2011; Cawthorn 2011). In fact, for the steady-state solution, Cawthorn (2011, p. 49) had already given an asymptotic solution for the wall speed \tilde{u}_w^∞ when the applied shear stress is just above the yield shear, i.e. when $\mu(\tilde{y} = 0, \tilde{t})$ approaches μ_s from above (or $\tilde{\mu}_w \sim 1$). However, it is also possible to obtain expressions for \tilde{u}_w^∞ for a wide range of $\tilde{\mu}_w$ via the self-similar solution (3.3) since, as suggested by figure 4, this gives a good approximation to the steady-state wall speed. In the limit when $\tilde{t} \gg 1$, the approximate solution (3.3) becomes a function only of \tilde{y} , and so, in terms of the normalised friction coefficient (3.9), it is given by $\tilde{\mu} \sim \tilde{\mu}_w + (1 - \tilde{\mu}_w)\tilde{y}$. Using this expression in (3.10), it reads

$$\tilde{u}_w^\infty \sim \int_0^1 \frac{\sqrt{1 + \beta_w \tilde{y}}}{\Delta\mu} \left(\frac{1}{\tilde{\mu}_w + (1 - \tilde{\mu}_w)\tilde{y}} - 1 \right) d\tilde{y}, \tag{3.11}$$

and since $\beta_w = (\mu_w/\mu_s - 1) < 1$, it could be further developed to obtain a simple expression for the steady-state wall velocity

$$\tilde{u}_w^\infty \sim -\frac{1}{\Delta\mu} \left[1 + \frac{\log \tilde{\mu}_w}{(1 - \tilde{\mu}_w)} \right] + O(\beta_w). \tag{3.12}$$

Noting that $\tilde{\mu}_w = 1 - \mu_s\beta_w/\Delta\mu$, it is straightforward to see that the first term in the above expression cancels out when $\tilde{\mu}_w \sim 1$ (or $\beta_w = (\mu_w/\mu_s - 1) \ll 1$), and thereby, it gives $\tilde{u}_w^\infty \sim O(\beta_w)$. In this case, as already deduced by Cawthorn (2011, p. 49), the

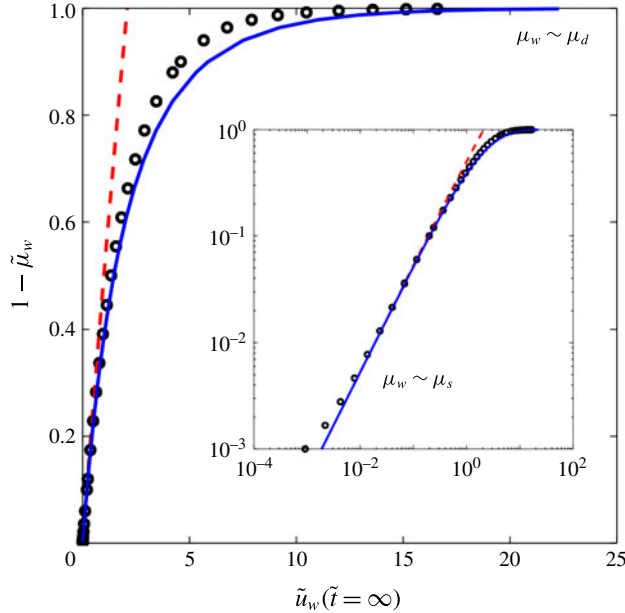


FIGURE 5. (Colour online) Comparison between direct computations and approximate expressions of the steady-state wall speed $\tilde{u}_w^\infty = \tilde{u}(\tilde{y} = 0, \tilde{t} \gg 1)$ as a function for the entire range of normalised wall friction coefficient $\tilde{\mu}_w = (\mu_d - \mu_w)/(\mu_d - \mu_s)$. Black circles denote the numerical solution using (2.15). The continuous line (blue) and the dashed line (red) are obtained using the expressions (3.12) and (3.13), respectively. The latter gives a good match when the applied shear stress is just above the yield shear stress $\tilde{\mu}_w \sim 1$ (or $\mu_w \sim \mu_s$), whereas the former captures the trend for all values of $\tilde{\mu}_w \in [0, 1]$.

above integral leads to

$$\tilde{u}_w^\infty \sim \frac{\mu_s}{2\Delta\mu^2} \left(\beta_w - \frac{5}{2}\beta_w^2 + O(\beta_w^3) \right). \tag{3.13}$$

For the case when $\tilde{\mu}_w$ tends to zero (or $\mu \rightarrow \mu_d$), the integral (3.11) will exhibit a logarithmic singularity at $\tilde{y} = 0$, and so $\tilde{u}_w^\infty \sim -\log \tilde{\mu}_w/\Delta\mu$. For the sake of completeness, it is pointed out that, even when β_w is not smaller than one, an expression similar to (3.12) could be developed at $\tilde{\mu}_w \ll 1$ by exploiting the logarithmic singularity in the integral (3.11).

The expressions (3.12) and (3.13) for \tilde{u}_w^∞ can now be verified by plotting the steady-state wall speed with respect to the normalised wall friction coefficient $\tilde{\mu}_w$ as in figure 5. Here, the exact wall speed (open circles) is computed by substituting the steady-state solution (2.10) in (3.10) and integrating it numerically. The asymptotic results (3.12) and (3.13) are displayed as continuous (blue) and dashed (red) lines, respectively. The normalised wall velocity varies slowly with the normalised friction coefficient $\tilde{\mu}_w$ as long as $1 - \tilde{\mu}_w$ is small (or $\mu_w \sim \mu_s$). Thus, for a given normal stress p_w at the wall, \tilde{u}_w varies linearly with the applied shear stress $\tau_w = \mu_w p_w$ if the latter is sufficiently close to the yield shear stress $\tau_s = \mu_s p_w$. Then the wall velocity increases rapidly with $1 - \tilde{\mu}_w$ and it becomes logarithmically large as μ_w approaches μ_d . This is not surprising since when τ_w approaches $\mu_d p_w$, the inertial

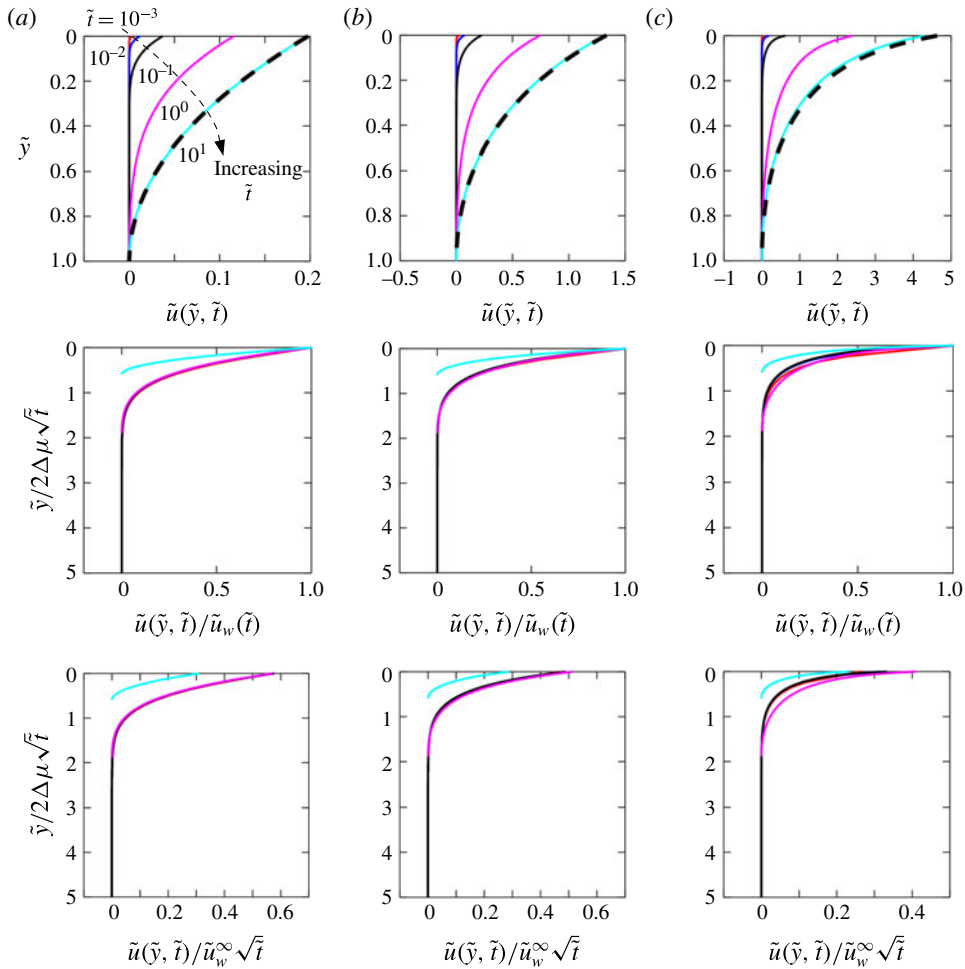


FIGURE 6. (Colour online) Velocity profile at different times $\tilde{t} = 10^{-3}, 10^{-2}, 10^{-1}, 10^0$ in the shear layer for various normalised wall friction coefficients $\tilde{\mu}_w = 0.9$ (a), $\tilde{\mu}_w = 0.5$ (b) and $\tilde{\mu}_w = 0.1$ (c). The thick dashed line represents the steady-state solution. These data are obtained by directly integrating the numerical solution of the non-dimensional shear-stress equation (2.15). The data collapse features in the second and third rows imply that the $\tilde{u}(\tilde{y}, \tilde{t}) \sim \tilde{u}_w^\infty \sqrt{\tilde{t}} f(\tilde{y}/2\Delta\mu\sqrt{\tilde{t}})$, where \tilde{u}_w^∞ is given by the expression (3.12).

number satisfies $I \gg 1$ in such a manner that frictional grain–grain contacts become less dominant compared to grain–grain collisions, as internal grain rearrangements are very frequent compared to the local deformation rate (Andreotti *et al.* 2011). Thus, a highly agitated flow can occur near the wall. Indeed, beyond this critical value, there is no longer an equilibrium between the applied shear stress and the internal resistance via frictional contacts as previously pointed out by Cawthorn (2011). A more relevant description is given by models inspired by the kinetic theory of gases (Jenkins & Savage 1983; Goldhirsch 2003). Furthermore, figure 5 indicates that the expression (3.13) provides a very good approximation to the steady-state wall speed when the applied shear stress is just above the yield stress $\tau_s = \mu_s p_w$ and the

expression (3.12) remarkably captures the wall speed variation for all applied shear stresses $\tau_w = \mu_w p_w \in [\mu_s p_w, \mu_d p_w]$.

The above result that the wall speed $\tilde{u}_w(\tilde{t}) \propto \sqrt{\tilde{t}}$ along with the fact that $\tilde{u}_w(\tilde{t} \gg 1)$ follows a universal trend (3.12) suggests that the velocity profile can be approximately deduced from the short-time asymptotic solution (3.3). This hypothesis is explored in figure 6, which shows three different normalisations of the velocity field as a function of time. Each column corresponds to specific wall boundary conditions corresponding to $\tilde{\mu}_w = 0.9$ (a), $\tilde{\mu}_w = 0.5$ (b) and $\tilde{\mu}_w = 0.1$ (c). The steady-state solution is displayed as a thick dashed line only in the first row but it is left out in the rest of the graphs for the sake of clarity. In this row, all figures present the time development of the velocity $\tilde{u}(\tilde{y}, \tilde{t})$ as computed by numerically integrating (3.10) at each $\tilde{t} = 10^{-3}, 10^{-2}, 10^{-1}, 10^0, 10^1$. As seen before in figure 4, it can be readily observed that the wall velocity $\tilde{u}(\tilde{y} = 0, \tilde{t})$ increases in time and attains a steady-state value which in turn depends on the applied wall shear stress. The numerical solution at $\tilde{t} = 10^1$ is already superimposed on the steady-state solution (dashed line) for all the cases of $\tilde{\mu}_w$ shown here. The second and the third rows in figure 6 display the same data when the velocity field is normalised with the wall speed $\tilde{u}_w(\tilde{t}) = \tilde{u}(\tilde{y} = 0, \tilde{t})$ and $\tilde{u}_w^\infty \sqrt{\tilde{t}}$, respectively, as a function of $\tilde{y}/2\Delta\mu\sqrt{\tilde{t}}$. Note that \tilde{u}_w^∞ is taken from the expression (3.12). Irrespective of the velocity normalisation, all the velocity profiles collapse onto a unique curve except for the cases when $\tilde{t} > O(1)$, as expected from the previous results. However, the collapse is only marginally good when $\tilde{\mu}_w = 0.1$ when $\tilde{t} \sim O(1)$ or greater. This implies that this observation may apply at shorter and shorter times as μ_w tends towards μ_d . Nonetheless, as long as $\tilde{t} \leq O(1)$, the velocity field should be given by $\tilde{u}(\tilde{y}, \tilde{t}) \sim \tilde{u}_w^\infty \sqrt{\tilde{t}} f(\tilde{y}/2\Delta\mu\sqrt{\tilde{t}})$, where \tilde{u}_w^∞ is given by the expression (3.12).

3.4. Stokes' first problem with imposed wall velocity

So far in this article Stokes' first problem has been considered for the case when the wall shear stress τ_w is imposed externally. Therefore, the wall velocity developed with time and, as the internal resistance of the granular medium balances out the applied stresses, it saturated to a constant value u_w . In contrast, it should be possible to set the granular medium in motion by imposing the wall speed u_w . Here, the resulting shear stress experienced by the wall should vary temporally as the internal resistance of the granular medium develops with time. However, it should also ultimately saturate to a constant value τ_w so that it gives precisely the same steady-state solution as for the imposed shear-stress case. In this subsection, a brief note on this variant of Stokes' first problem is presented.

As already seen in figure 5, in the steady-state solution, for each wall friction coefficient there exists one and only one wall velocity. Therefore, it is reasonable to leave the normalised variables of the previous sections as such. Now by using the normalised local friction coefficient $\tilde{\mu} = (\mu_d - \mu)/\Delta\mu$, (3.1) can be rewritten as

$$\frac{\partial \tilde{\mu}}{\partial \tilde{t}} = \Delta\mu^2 \tilde{\mu}^2 \left(\frac{2\beta_w}{\sqrt{1 + \beta_w \tilde{y}}} \frac{\partial \tilde{\mu}}{\partial \tilde{y}} + \sqrt{1 + \beta_w \tilde{y}} \frac{\partial^2 \tilde{\mu}}{\partial \tilde{y}^2} \right), \tag{3.14}$$

which for the case of Stokes' first problem with imposed wall velocity should satisfy the initial condition $\tilde{\mu}(\tilde{y}, \tilde{t} = 0) = 1$ (or $\mu = \mu_s$) along with the boundary conditions

$$\tilde{u}_w = \int_0^1 \frac{\sqrt{\tilde{p}}}{\Delta\mu} \left(\frac{1}{\tilde{\mu}} - 1 \right) d\tilde{y}, \tag{3.15}$$

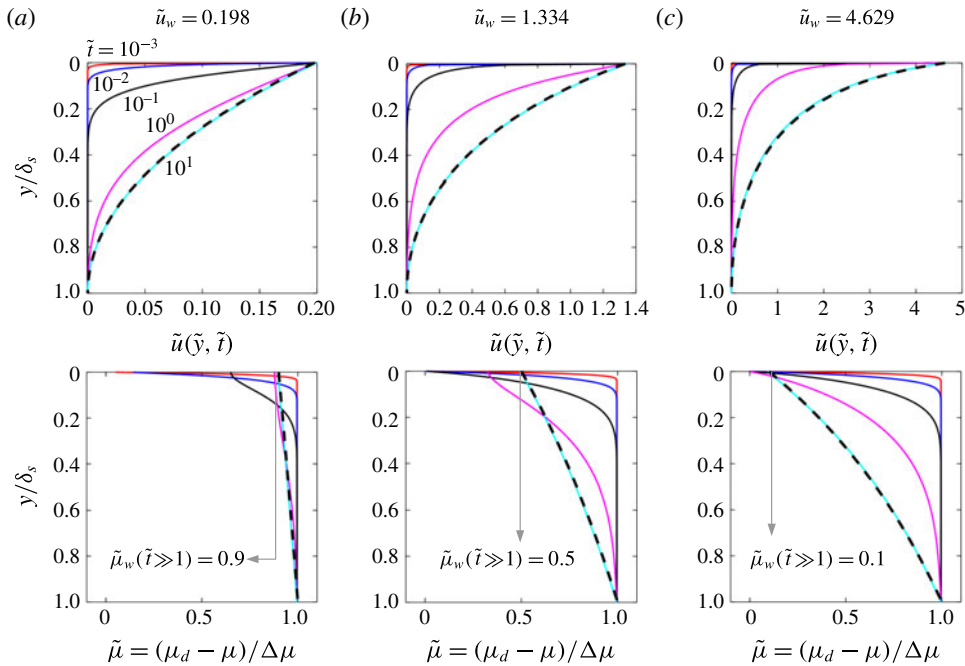


FIGURE 7. (Colour online) Numerical results for Stokes' first problem with imposed wall velocity showing the evolution of the velocity $\tilde{u}(\tilde{y}, \tilde{t})$ (top) and the normalised friction coefficient $\tilde{\mu}(\tilde{y}, \tilde{t})$ (bottom) at different times $\tilde{t} = 10^{-3}, 10^{-2}, 10^{-1}, 10^0, 10^1$ for various imposed wall speeds \tilde{u}_w . These data are obtained by directly integrating the numerical solution of the non-dimensional shear-stress equation (3.14) with the wall boundary condition (3.15). The thick dashed line represents the steady-state solution. The imposed wall speed \tilde{u}_w was chosen to match with the steady-state wall speed in figure 6.

and $\tilde{\mu}(\tilde{y} = 1, \tilde{t}) = 1$. Here, the initial and lower boundary conditions are chosen so as to satisfy $\tilde{u} = 0$, which is possible only when $\mu = \mu_s$ in the $\mu(I)$ -rheology. The integral condition imposes the wall velocity on the choice of the vertical distribution of the normalised local friction coefficient $\tilde{\mu}$. In particular, note that the parameter $\beta_w = \phi \rho g \delta_s / p_w$ as in (2.11) since the steady-state solution (2.10) for Stokes' first problem with applied shear stress should also apply to this case where the wall speed is externally imposed. Thus $\beta_w = \mu_w^\infty / \mu_s - 1$, where μ_w^∞ is the steady-state wall friction coefficient that is needed to sustain the applied wall speed u_w .

Figure 7 presents the velocity $\tilde{u}(\tilde{y}, \tilde{t})$ (top) and the normalised friction coefficient $\tilde{\mu}(\tilde{y}, \tilde{t})$ (bottom) profiles that are obtained by numerically solving (3.14) for $\tilde{\mu}$ satisfying the imposed wall velocity condition as given by (3.15). Each continuous line represents a different time as indicated in the figure ($\tilde{t} = 10^{-3}, 10^{-2}, 10^{-1}, 10^0, 10^1$) and the thick dashed line represents the steady-state solution. Note that particular wall speeds ((a) $\tilde{u}_w = 0.198$, (b) $\tilde{u}_w = 1.334$ and (c) $\tilde{u}_w = 4.629$) were chosen so that the resulting steady-state velocity and local friction coefficient profiles are the same as that obtained in figure 6 for the case when wall shear stress is imposed. As expected, in all figures, the velocity profile (top) and the related boundary layer develops with time in such a way that the velocity at the wall is equal to the applied wall speed \tilde{u}_w at all times, and the size of the mobile layer increases until approximately $\tilde{t} \sim O(1)$. This is true for the normalised wall friction coefficient (bottom) as well. Also, both

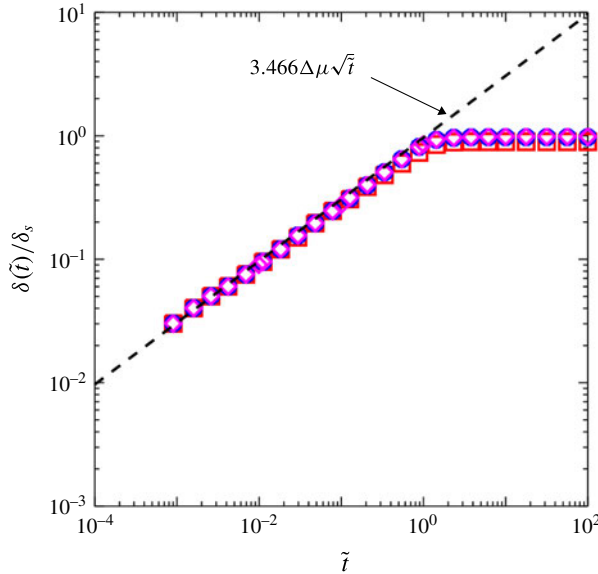


FIGURE 8. (Colour online) Temporal evolution of the shear layer thickness δ/δ_s for the profiles presented in figure 7. Different symbols correspond to various imposed wall velocities (\square , $\tilde{u}_w = 0.198$; \circ , $\tilde{u}_w = 1.334$; \diamond , $\tilde{u}_w = 4.629$). As already seen in figure 2 (bottom) for the case when the wall shear stress is imposed, the shear layer grows as $\sqrt{\tilde{t}}$ until approximately $\tilde{t} \sim O(1)$.

$\tilde{u}(\tilde{y}, \tilde{t})$ and $\tilde{\mu}(\tilde{y}, \tilde{t})$ match with their respective steady-state profiles (thick dashed line) for sufficiently large time $\tilde{t} > O(1)$.

With these data, it is then possible to calculate the size of the mobile layer, say $\delta(\tilde{t})$, where the local shear stress is just above the threshold shear $\tau_s = \mu_s p$. Figure 8 illustrates that $\delta(\tilde{t})$ increases with time as $\sqrt{\tilde{t}}$ until $\tilde{t} \sim O(1)$, after which it saturates to the steady-state limit. Even though this is similar to what was observed previously for the case of Stokes’ problem when the wall shear is imposed, as seen in figure 2 (bottom), the evolution of the wall friction coefficient $\mu_w(\tilde{t})$ takes place in two stages (see figure 9). It is observed that $\mu_w(\tilde{t})$ is close to μ_d for sufficiently small times, say up to when $\tilde{t} \leq \tilde{t}_{\mu d}$. Then it decreases as $1/\sqrt{\tilde{t}}$ until it attains the steady state at $\tilde{t} \sim \tilde{t}_{\mu w}$. Thus, the corresponding wall shear stress $\tau_w(\tilde{t}) = \mu_w(\tilde{t})p_w$ initially remains sufficiently close to the critical shear stress $\mu_d p_w$ before decreasing monotonically towards the wall shear stress that is needed to sustain the applied wall velocity \tilde{u}_w . It suggests that the time at which these two stages occur should depend on \tilde{u}_w and these time scales are different from δ_s^2/ν_g .

For $\tilde{t}_{\mu d} \leq \tilde{t} \leq \tilde{t}_{\mu w}$, an order of magnitude analysis of (2.5) gives $u_w/t \sim (\mu_w(t) - \mu_s)p_w/\delta(t)$. In terms of the non-dimensional time \tilde{t} and wall velocity \tilde{u}_w , this can be rewritten as

$$\mu_w(\tilde{t}) - \mu_s \sim \frac{\tilde{u}_w}{3.66\Delta\mu\sqrt{\tilde{t}}}, \tag{3.16}$$

since $\delta \sim 3.66\Delta\mu\sqrt{\tilde{t}}$ as shown by figure 8. Since when $\tilde{t} \sim \tilde{t}_{\mu d}$, $\mu_w(\tilde{t}) - \mu_s \approx \Delta\mu$, this implies that the wall friction coefficient should be around μ_d until some time

$$\tilde{t}_{\mu d} \propto \tilde{u}_w^2. \tag{3.17}$$

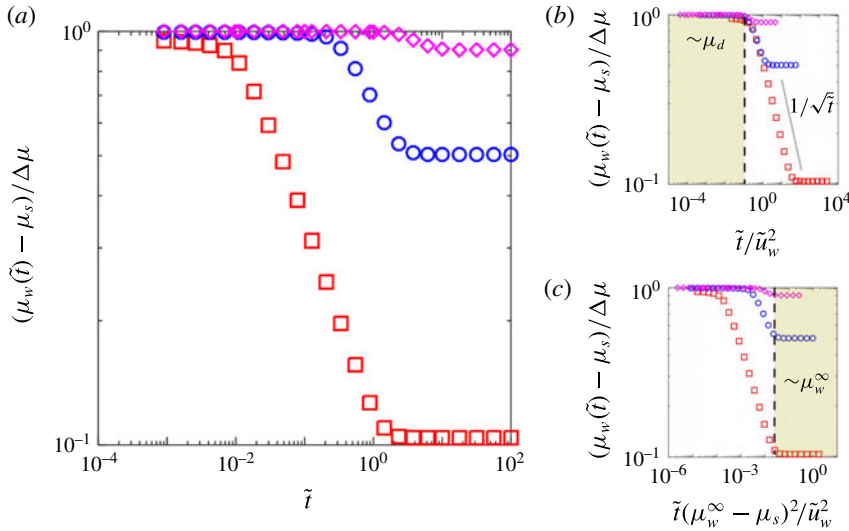


FIGURE 9. (Colour online) Evolution of the wall friction coefficient $\mu(\tilde{y} = 0, \tilde{t}) = \mu_w(\tilde{t})$ for various imposed wall velocities (\square , $\tilde{u}_w = 0.198$; \circ , $\tilde{u}_w = 1.334$; \diamond , $\tilde{u}_w = 4.629$). Figures on the right display the same data as a function of two different normalisations of the time variable based on the scaling laws (3.17) and (3.18).

Thus, according to $\mu(I)$ -rheology, in order to sustain an applied wall speed \tilde{u}_w with the no-slip condition, the granular medium develops a strong shear stress (about $\mu_d p_w$) near the wall for all times $\tilde{t} \leq \tilde{t}_{\mu d}$. From this point onwards, the wall shear stress should decrease monotonically as $1/\sqrt{\tilde{t}}$ until the local friction coefficient (or the local shear stress) distribution has reached the steady-state solution to give $\mu_w(\tilde{t} \gg 1) = \mu_w^\infty$. Here, μ_w^∞ is a function of the applied wall speed and it can be either estimated directly by integrating the steady-state profile (2.10) or approximately via the expression (3.12). Using (3.16), it is seen that the wall friction coefficient, and hence the wall shear stress, should attain a steady-state value at some time

$$\tilde{t}_{\mu w} \propto \left(\frac{\tilde{u}_w}{\mu_w^\infty - \mu_s} \right)^2. \tag{3.18}$$

These two time scales can be verified by plotting the data from figure 9(a) as a function of properly rescaled time with respect to the relations (3.17) and (3.18). This is done in figure 9 (see plots b,c) where the data collapse indicates a good agreement with the above scaling laws.

Finally, an approximate expression can now be elaborated for $\mu(\tilde{y}, \tilde{t})$ due to the fact that the shear layer $\tilde{\delta}$ is small up to $\tilde{t} \sim O(1)$. As done before in § 3.1, (3.14) becomes

$$\frac{\partial \tilde{\mu}}{\partial \tilde{t}} = (\Delta \mu^2 \tilde{\mu}^2) \frac{\partial^2 \tilde{\mu}}{\partial \tilde{y}^2}, \tag{3.19}$$

at short time \tilde{t} . This equation is singular near the wall region $\tilde{y} \ll 1$ since $\tilde{\mu} \sim 0$ at least until $\tilde{t}_{\mu d}$ (see figure 9). Nonetheless, the chosen initial condition $\tau(\tilde{y}, t=0) = \mu_s p$ implies that there exists a zone where $\mu \sim \mu_s$ (or $\tilde{\mu} \sim 1$) away from the wall until the

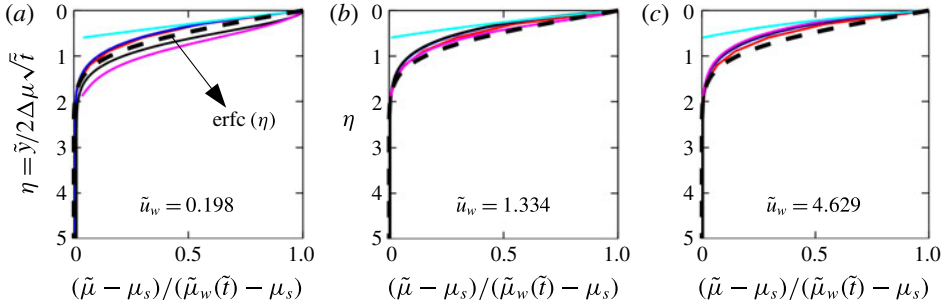


FIGURE 10. (Colour online) The same data as in figure 7 (bottom) for different times $\tilde{t} = 10^{-3}, 10^{-2}, 10^{-1}, 10^0, 10^1$ but plotted here against the self-similar variable $\eta = \tilde{y}/2\Delta\mu\sqrt{\tilde{t}}$. A reasonably good collapse is observed.

shear layer is completely developed, i.e. for all $\tilde{t} \leq O(1)$. In this outer zone $\Delta\mu\tilde{\mu} \sim \Delta\mu$ and hence the above equation reduces to a simple diffusion equation wherein the outer solution should be $\mu = \mu_s + A \operatorname{erfc}(\tilde{y}/2\Delta\mu\sqrt{\tilde{t}})$. Here A is an arbitrary constant that could be deduced by matching this solution to the inner region where the friction coefficient $\tilde{\mu} \sim 0$. Here, $\mu \sim \mu_w(\tilde{t})$ and therefore

$$\mu(\tilde{y}, \tilde{t}) = \mu_s + (\mu_w(\tilde{t}) - \mu_s) \operatorname{erfc}\left(\frac{\tilde{y}}{2\Delta\mu\sqrt{\tilde{t}}}\right) \tag{3.20}$$

is obtained as an approximate expression for the friction coefficient $\mu(\tilde{y}, \tilde{t})$ as long as \tilde{t} is sufficiently small. When this expression is compared with the numerical results (see figure 10) a reasonable fit is observed for all $\tilde{t} \leq O(1)$. As previously shown from computational data in figure 9, it is pointed out here that $\mu_w(\tilde{t}) - \mu_s \sim \Delta\mu$ for all $\tilde{t} \leq \tilde{t}_{\mu d}$ and $\mu_w(\tilde{t}) - \mu_s \sim \tilde{u}_w/\Delta\mu\sqrt{\tilde{t}}$ when $\tilde{t}_{\mu d} \leq \tilde{t} \leq \tilde{t}_{\mu w}$.

4. Conclusion

Using the $\mu(I)$ -rheology, the so-called Stokes’ first problem on the motion of a granular liquid set up by an impulsively started flat plate is studied both numerically and theoretically. The problem is first well-posed in terms of a nonlinear diffusion equation for the local shear stress with proper initial and boundary conditions in order to avoid the Hadamard instability. Numerical solutions are then obtained for both externally imposed wall stress and speed. Approximate solutions at short and long times are also illustrated to capture the main features of the numerical results.

For the case when the dense granular flow is brought about by applying constant shear stress τ_w at $t > 0$, if τ_w is greater than the yield stress at the wall $\mu_s p_w$ (where p_w is the applied pressure at the wall) then the $\mu(I)$ -rheology implies that it is diffused into the granular medium until the shear stress is uniform throughout the medium such that, at any time t , the applied shear stress reaches a depth proportional to $\sqrt{v_g t}$ where $v_g = (d/2\phi\Delta\mu I_0)\sqrt{p_w/\rho}$ denotes the diffusion coefficient for the local shear stress. A steady state, wherein a finite zone of grains (of thickness, say, δ_s) yield, and hence flow, due to the applied shear, is thus shown to occur at a finite time of the approximate order δ_s^2/v_g . Here, if $\beta_w = (\mu_w - \mu_s)/\mu_s$, the shear layer depth δ_s is $\beta_w p_w / \phi \rho g$ as already obtained by Andreotti *et al.* (2011) and Cawthorn (2011). If the

no-slip condition is allowed, the wall velocity develops in time as $u_w^\infty \sqrt{v_g t} / \delta_s$ until approximately a time $t \sim O(\delta_s^2 / v_g)$.

If the dense granular flow is set up by suddenly imparting a constant speed u_w on the wall at $t > 0$, the internal resistance of the medium develops in a small region close to the wall and later it is diffused into the shear layer. As a result, the $\mu(I)$ -rheology suggests that, initially when the wall is set in motion, the shear stress experienced by the granular medium in the neighbourhood of the velocity-driven wall should be sufficiently close to the critical shear stress $\tau_d = \mu_d p_w$ until some time $t_{\mu d}$ proportional to $v_g (u_w / g \delta_s)^2$. Thereafter, the wall shear stress τ_w decreases with time as a power law $1/\sqrt{t}$ before reaching its steady-state value necessary to support the externally imposed wall speed u_w . At this stage the shear stress becomes uniform in the bulk of the mobile layer.

In both variants of Stokes' problem in granular media, a properly rescaled friction coefficient (or the shear stress) is illustrated to be approximately self-similar with respect to the variable $y/\Delta\mu\sqrt{v_g t}$. Moreover, the steady-state wall speed, wall shear stress and the applied wall pressure are related by a simple approximate expression (3.12) which in terms of dimensional parameters can be given as $u_w \sim (g\delta_s^2/v_g)f(\beta_w)$, where $f(\beta_w)$ is a function of the surplus steady-state wall shear stress $\beta_w = (\tau_w - \mu_s p_w)/\mu_s p_w$ such that it is either $O(1)$ when the wall shear stress is just above the yield stress $\tau_w \sim \tau_s$ or logarithmically large as τ_w approaches τ_d .

Note that when the local friction coefficient μ approaches μ_d , the local inertial number, which compares the time scale of grain–grain rearrangements with that arising from the macroscopic deformation of the medium, should be very large ($I \gg 1$). Therefore, the aforementioned result that, for $t \leq t_{\mu d}$, the local shear stress $\tau = \mu p$ tends towards $\tau_d = \mu_d p$ in the immediate vicinity of the region where velocity is imposed, suggests that a highly agitated granular flow could occur in this zone. A viscoplastic description of the $\mu(I)$ -rheology might, in fact, not be suitable in such zones as the local shear stress therein cannot be supported by internal grain–grain frictional resistance alone. Here, a proper model for rapid granular flows (Jenkins & Savage 1983; Goldhirsch 2003) should be more pertinent. Furthermore, if the applied wall speed u_w is much larger than $v_g/g\delta_s^2$ so that $t_{\mu d}$ becomes sufficiently large, the resulting unsteady granular flow as computed from the $\mu(I)$ -rheology may even be incorrect.

It is expected that this study will motivate investigations of the further validity of the $\mu(I)$ -rheology for unsteady dense granular flows using simple experiments. These results should also be helpful to better understand shear layers, effective viscosity, drag force and characteristic diffusion time scales in future studies with the $\mu(I)$ -rheology. Especially in the context of the ill-posedness of the $\mu(I)$ -rheology as an initial-value problem, it might be essential to identify what features predicted by this rheology are still meaningful. It will be of some interest to include the spatio-temporal variation of the solid fraction ϕ as well – via, for example, a linear function of the inertial number I as in Jop *et al.* (2006). Non-local effects by which a granular medium can yield even if the local shear stress is below the yield criterion are omitted in the present short note for the sake of simplicity, but they might play an important role under common experimental conditions. Finally, it is pointed out that Stokes' second problem with an oscillating wall boundary condition remains a very interesting open problem, as it might shed light on how static and dynamic zones can simultaneously appear and move around in unsteady flow fields predicted by the $\mu(I)$ -rheology of dense granular flows. However, the $\mu(I)$ -rheology can neither account for the history of the shear stress in the bulk of the medium nor consider other static initial

conditions that are different from the yield criterion. It is nonetheless important to study these configurations using the $\mu(I)$ -rheology to further advance knowledge about continuum models for unsteady dense granular flows.

Acknowledgements

The authors acknowledge vital inputs from S. Dagois Bohy and all correspondences with D. Doppler and P. Jop.

REFERENCES

- ANCEY, C. & BATES, B. M. 2017 Stokes' third problem for Herschel–Bulkley fluids. *J. Non-Newtonian Fluid Mech.* **243** (Supplement C), 27–37.
- ANCEY, C., COUSSOT, P. & EVESQUE, P. 1999 A theoretical framework for granular suspensions in a steady simple shear flow. *J. Rheol.* **43** (6), 1673–1699.
- ANDREOTTI, B., FORTERRE, Y. & POULIQUEN, O. 2011 *Les milieux granulaires: entre fluide et solide*. EDP Sciences.
- ARANSON, I. S. & TSIMRING, L. S. 2006 Patterns and collective behavior in granular media: theoretical concepts. *Rev. Mod. Phys.* **78** (2), 641.
- BAKER, J. L., BARKER, T. & GRAY, J. M. N. T. 2016 A two-dimensional depth-averaged $\mu(I)$ -rheology for dense granular avalanches. *J. Fluid Mech.* **787**, 367–395.
- BALMFORTH, N. J., FORTERRE, Y. & POULIQUEN, O. 2009 The viscoplastic Stokes layer. *J. Non-Newtonian Fluid Mech.* **158** (1), 46–53.
- BARKER, T. & GRAY, J. M. N. T. 2017 Partial regularisation of the incompressible $\mu(I)$ -rheology for granular flow. *J. Fluid Mech.* **828**, 5–32.
- BARKER, T., SCHAEFFER, D. G., BOHORQUEZ, P. & GRAY, J. M. N. T. 2015 Well-posed and ill-posed behaviour of the $\mu(I)$ -rheology for granular flow. *J. Fluid Mech.* **779**, 794–818.
- BARKER, T., SCHAEFFER, D. G., SHEARER, M. & GRAY, J. M. N. T. 2017 Well-posed continuum equations for granular flow with compressibility and $\mu(I)$ -rheology. *Proc. R. Soc. A* **473**, 20160846.
- CAPART, H., HUNG, C.-Y. & STARK, C. P. 2015 Depth-integrated equations for entraining granular flows in narrow channels. *J. Fluid Mech.* **765**, R4.
- CAWTHORN, C. J. 2011 Several applications of a model for dense granular flows. PhD thesis, University of Cambridge.
- CHAUCHAT, J. & MÉDALE, M. 2014 A three-dimensional numerical model for dense granular flows based on the $\mu(I)$ -rheology. *J. Comput. Phys.* **256**, 696–712.
- DA CRUZ, F., EMAM, S., PROCHNOW, M., ROUX, J.-N. & CHEVOIR, F. 2005 Rheophysics of dense granular materials: discrete simulation of plane shear flows. *Phys. Rev. E* **72** (2), 021309.
- DEVAKAR, M. & IYENGAR, T. K. V. 2008 Stokes problems for an incompressible couple stress fluid. *Nonlinear Anal.: Model. Control* **1** (2), 181–190.
- DEVAKAR, M. & IYENGAR, T. K. V. 2009 Stokes' first problem for a micropolar fluid through state-space approach. *Appl. Math. Modell.* **33** (2), 924–936.
- EKINCI, K. L., KARABACAK, D. M. & YAKHOT, V. 2008 Universality in oscillating flows. *Phys. Rev. Lett.* **101**, 264501.
- FORTERRE, Y. & POULIQUEN, O. 2008 Flows of dense granular media. *Annu. Rev. Fluid Mech.* **40**, 1–24.
- GODDARD, J. D. & LEE, J. 2017 On the stability of the $\mu(I)$ rheology for granular flow. *J. Fluid Mech.* **833**, 302–331.
- GOLDHIRSCH, I. 2003 Rapid granular flows. *Annu. Rev. Fluid Mech.* **35** (1), 267–293.
- GRAY, J. M. N. T. & EDWARDS, A. N. 2014 A depth-averaged $\mu(I)$ -rheology for shallow granular free-surface flows. *J. Fluid Mech.* **755**, 503.
- GRAY, J. M. N. T., TAI, Y.-C. & NOELLE, S. 2003 Shock waves, dead zones and particle-free regions in rapid granular free-surface flows. *J. Fluid Mech.* **491**, 161–181.

- HUTTER, K. & RAJAGOPAL, K. R. 1994 On flows of granular materials. *Contin. Mech. Thermodyn.* **6** (2), 81–139.
- IORDANOFF, I. & KHONSARI, M. M. 2004 Granular lubrication: toward an understanding of the transition between kinetic and quasi-fluid regime. *J. Tribol.* **126** (1), 137–145.
- JAEGER, H. M., NAGEL, S. R. & BEHRINGER, R. P. 1996 Granular solids, liquids, and gases. *Rev. Mod. Phys.* **68** (4), 1259.
- JENKINS, J. T. & SAVAGE, S. B. 1983 A theory for the rapid flow of identical, smooth, nearly elastic, spherical particles. *J. Fluid Mech.* **130**, 187–202.
- JOP, P., FORTERRE, Y. & POULIQUEN, O. 2006 A constitutive law for dense granular flows. *Nature* **441** (7094), 727–730.
- JOP, P., FORTERRE, Y. & POULIQUEN, O. 2007 Initiation of granular surface flows in a narrow channel. *Phys. Fluids* **19** (8), 088102.
- JOSEPH, D. D. & SAUT, J. C. 1990 Short-wave instabilities and ill-posed initial-value problems. *Theor. Comput. Fluid Dyn.* **1** (4), 191–227.
- KAMRIN, K. 2010 Nonlinear elasto-plastic model for dense granular flow. *Intl J. Plast.* **26** (2), 167–188.
- LAGRÉE, P.-Y., STARON, L. & POPINET, S. 2011 The granular column collapse as a continuum: validity of a two-dimensional Navier–Stokes model with a $\mu(I)$ -rheology. *J. Fluid Mech.* **686**, 378–408.
- LIU, A. J. & NAGEL, S. R. 1998 Nonlinear dynamics: jamming is not just cool any more. *Nature* **396** (6706), 21–22.
- MARTIN, N., IONESCU, I. R., MANGENEY, A., BOUCHUT, F. & FARIN, M. 2017 Continuum viscoplastic simulation of a granular column collapse on large slopes: $\mu(I)$ rheology and lateral wall effects. *Phys. Fluids* **29** (1), 013301.
- MIDI, G. D. R. 2004 On dense granular flows. *Eur. Phys. J. E* **14** (4), 341–365.
- MORRISON, J. A. 1956 Wave propagation in rods of Voigt material and visco-elastic materials with three-parameter models. *Q. Appl. Maths* **14** (2), 153–169.
- PANTON, R. 1968 The transient for Stokes's oscillating plate: a solution in terms of tabulated functions. *J. Fluid Mech.* **31** (4), 819–825.
- PREZIOSI, L. & JOSEPH, D. D. 1987 Stokes' first problem for viscoelastic fluids. *J. Non-Newtonian Fluid Mech.* **25** (3), 239–259.
- PRITCHARD, D., MCARDLE, C. R. & WILSON, S. K. 2011 The Stokes boundary layer for a power-law fluid. *J. Non-Newtonian Fluid Mech.* **166** (12), 745–753.
- SAVAGE, S. B. 1984 The mechanics of rapid granular flows. *Adv. Appl. Mech.* **24**, 289–366.
- SCHLICHTING, H. 1968 *Boundary-Layer Theory*. McGraw-Hill.
- STARON, L., LAGRÉE, P.-Y. & POPINET, S. 2012 The granular silo as a continuum plastic flow: the hour-glass vs the clepsydra. *Phys. Fluids* **24** (10), 103301.
- STOKES, G. G. 1851 *On the Effect of the Internal Friction of Fluids on the Motion of Pendulums*. Pitt Press.
- TANNER, R. I. 1962 Note on the Rayleigh problem for a visco-elastic fluid. *Z. Angew. Math. Phys.* **13** (6), 573–580.
- THOMPSON, P. A. & GRETT, G. S. 1991 Granular flow: friction and the dilatancy transition. *Phys. Rev. Lett.* **67** (13), 1751.
- YAKHOT, V. & COLOSQUI, C. 2007 Stokes' second flow problem in a high-frequency limit: application to nanomechanical resonators. *J. Fluid Mech.* **586**, 249–258.